

Coordinate control strategy for stability operation of offshore wind farm integrated with Diode-rectifier HVDC

Lijun Xie¹, Liangzhong Yao², Fan Cheng^{1,2}, Yan Li¹, Shuai Liang²

1. China Electric Power Research Institute, Haidian District, Beijing 100192, P.R.China

2. School of Electrical and Electronic Engineering and Automation, Wuhan University, Wuchang District, Wuhan 430072, P.R. China



Scan for more details

Abstract: Due to low investment cost and high reliability, a new scheme called DR-HVDC (Diode Rectifier based HVDC) transmission was recently proposed for grid integration of large offshore wind farms. However, in this scheme, the application of conventional control strategies for stability operation face several challenges due to the uncontrollability of the DR. In this paper, a coordinated control strategy of offshore wind farms using the DR-HVDC transmission technology to connect with the onshore grid, is investigated. A novel coordinated control strategy for DR-HVDC is proposed based on the analysis of the DC current control ability of the full-bridge-based modular multilevel converter (FB-MMC) at the onshore station and the input and output characteristics of the diode rectifier at the offshore. Considering the characteristics of operation stability and decoupling between reactive power and active power, a simplified design based on double-loop droop control for offshore AC voltage is proposed after power flow and voltage–current (I – V) characteristics of the offshore wind farm being analyzed. Furthermore, the impact of onshore AC fault to offshore wind farm is analyzed, and a fast fault detection and protection strategy without relying on communication is proposed. Case studies carried out by PSCAD/EMTDC verify the effectiveness of the proposed control strategy for the start up, power fluctuation, and onshore and offshore fault conditions.

Keywords: Diode rectifier, HVDC, PMSG, FB-MMC, Control strategy, AC fault.

1 Introduction

The voltage source converter based on high-voltage direct current (VSC-HVDC) transmission technology has

attracted increasing attention because of its advantages such as flexible control, supply to passive system, and the need for few filter banks; further, it has gained popularity for use in offshore wind farm integration [1–2]. The AC voltage control of offshore wind farm is important to ensure the transmission of offshore wind power, and it is controlled by the rectifier converter at the transmission end in the VSC-HVDC schemes [3–6]. An alternative control strategy for offshore voltage control is proposed, wherein a voltage control strategy developed in a microgrid [7–12] is applied to wind turbines, which enables the wind turbines to operate as grid forming units and provide voltage and frequency control [13–15]. However, when the wind turbines operate

Received: 5 January 2020/ Accepted: 20 March 2020/ Published: 25 June 2020

✉ Lijun Xie
lijun-xie@163.com

Liangzhong Yao
yao.liangzhong@whu.edu.cn

Fan Cheng
chengfan5566@163.com

Yan Li
liyan@epri.sgcc.com.cn

Shuai Liang
liangshuai93@163.com

in a grid forming unit, it is difficult to achieve the maximum power tracking without auxiliary components.

Recently, a new topology called DR-HVDC transmission was proposed to deal with offshore wind farm integration with advantage of low cost and high reliability [16–17]. The wind farm can operate at maximum power point tracking without auxiliary components when the DR topology is combined with the voltage control strategy of wind turbines. Different strategies have been proposed for wind turbine control, including centralized control [17–19], synchronous control based on GPS signals [20–21], master-slave control [22–24], and droop control [25–27], which are similar to strategies developed in the micro grid.

The droop control used in [25–27], which uses the local signal and achieves hot-plug, is more easy to implement [7–9]. However, the droop control methods utilize P–V and Q–f droop characteristics to control active and reactive power flows, and they are characterized by slow dynamics and the coupling of active and reactive power. Droop control is divided into single-loop droop control and multi-loop droop control [7–9]. The latter is prone to being less damped and experiencing instability more easily especially in a high-power converter, with negative damping synthesized by the inner current loop at certain harmonic frequencies [25–26]. Therefore, multi-loop control schemes can hardly meet the requirement of voltage waveform quality.

In the DR-HVDC transmission scheme, the onshore converter operates as a voltage source, and the wind farm and rectifier operate as a current source [17–27]. However, this coordinated control is problematic once a DC fault occurs, and an additional control strategy or equipment is required.

The linear relationship of diode rectifier between the input and output and DC current control ability of the onshore converter is analyzed, and it provides new insight

into the control of the DR-HVDC system. A coordinate control strategy is proposed for DR-HVDC system. With DC current being controlled by onshore converter and power flow analysis of offshore wind farm, a simplified control strategy for wind turbines based on I–V droop characteristics is designed and analyzed with the stability improvement of the AC voltage of offshore wind farms, which also decouples the active and reactive power. A new insight of frequency control is proposed based on Park transmission. A current-error-dependent fault protection is used to protect converters from the overcurrent via regulation of the voltage of the wind turbine during fault transients because the inner current loop is eliminated. The proposed control strategy allows for the synchronization of wind turbines, reactive power sharing without communications between wind turbines, fast response once fault occurs, and fast recovery after the fault is cleared.

The remainder of this manuscript is organized as follows: The mathematic model in the dq axis of the offshore wind power system is presented in Section 2. A simplified voltage controller based on I–V droop characteristics is proposed with protection schemes in Section 3. Section 4 presents the simulation model built in PSCAD/EMTDC to verify the controller. Finally, the conclusions of this study are provided in Section 5.

2 Model of the offshore wind farm and DR-HVDC

The offshore wind farm collected by DR is shown in Fig. 1, and it consists of several wind turbine (WT) clusters. Each cluster comprises fully rated converter-based WTs. The offshore AC grid is connected to the offshore DC grid with a 12-pulse diode rectifier that comprises two 6-pulse diode bridges, thereby enabling better power quality at the

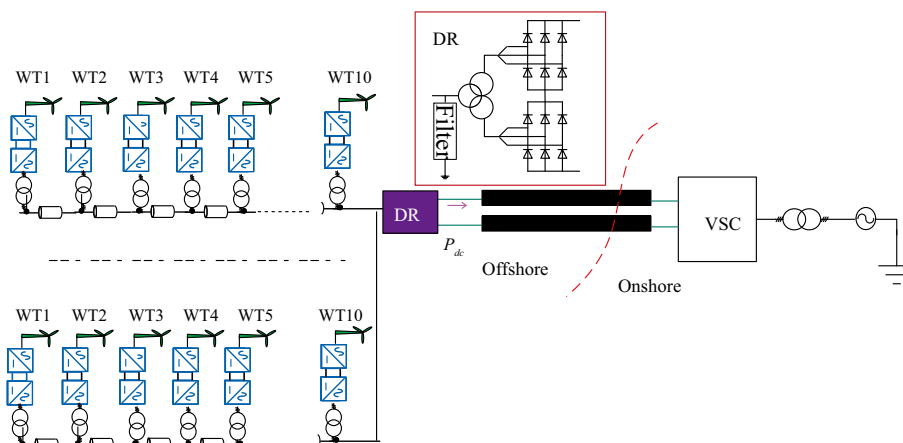


Fig. 1 Topology of wind farm integrated by diode-based rectifier

collection point of the AC grid. Further, reactive power compensation and harmonic filtering is achieved by the capacitor and filter banks. The pulse of the diode rectifier can be increased to cut the weight and size of platform further because the volume of the harmonic filters is less; however, it will increase the difficulty of transformer design and investment. Only a 12-pulse diode rectifier is used in this paper.

The MMC technique is selected for future VSC-based HVDC grids. The FB-MMC not only can block DC faults but also provide flexible control because of the negative voltage generating capability [5–6]; it is used in this study.

Following the criterion of connecting the wind farms into power grid, the wind power system should provide active power and reactive power control. A permanent magnet synchronous generator (PMSG) is used as the wind turbine generator, cascaded with a fully rated AC/DC rectifier as machine side converter (MSC) and a DC/AC inverter as grid side converter (GSC) based on IGBT. Unlike a conventional wind power system, the GSC needs to achieve the control of AC voltage at the collection point, as the rectifier station cannot control the AC voltage of offshore wind farms. To maintain the power balance of wind power system, the MSC of wind turbine is used to control the DC link voltage.

2.1 Onshore converter based on FBMMC

The diagram of FBMMC is shown in Fig. 2; FBMMC is composed of six arms, and each arm includes 2N sub-models and arm inductors L_s . v_{ap} and v_{an} are the

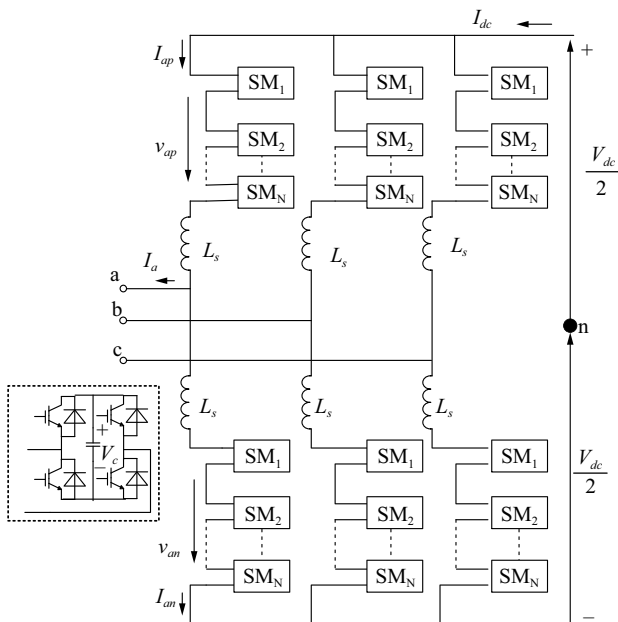


Fig. 2 Diagram of FBMMC

output voltages of the upper and lower arms of phase A, respectively, and i_{ap} and i_{an} are the currents of the upper and lower arms of phase A, respectively.

As the output voltage of the sub-model of FB-MMC can be $-v_c$, 0, and $+v_c$, DC voltage of FB-MMC can be controlled from V_{dc} to $-V_{dc}$ [28–31], making the FB-MMC can be in current source converter mode or an voltage source converter. Consider the output voltage of phase A as an example.

$$\begin{cases} v_{ap} = \frac{V_{dc}}{2} - u_a - \frac{u_{acm}}{2} \\ v_{an} = \frac{V_{dc}}{2} + u_a - \frac{u_{acm}}{2} \end{cases} \quad (1)$$

where u_a is the AC voltage of the FB-MMC, V_{dc} is DC voltage of the FB-MMC, and u_{acm} is the common-mode voltage used to control the circulation current.

From the DC side, according to KVL

$$\frac{2L_s}{3} \frac{di_{dc}}{dt} = V_{dc} - \sum_{a,b,c} \sum_{p,n} \sum_1^N v_c \quad (2)$$

The dc-link dynamic can be directly controlled by controlling sub-model capacitor voltage.

2.2 Offshore rectifier based on diode

The relationship of the average DC voltage of the diode-based bridge V_{Rdc} and the AC voltage V_F and DC current I_{dc} is

$$\begin{cases} V_{Rdc} = \frac{3\sqrt{6}}{\pi} B N V_F - \frac{3}{\pi} B \omega_F L_{TR} I_{dc} \\ V_{Rdc} = V_{dc} + I_{dc} R \end{cases} \quad (3)$$

where L_{TR} is the reactance of the diode rectifier transformer, ω_F is the frequency of the offshore system, V_{dc} is the DC voltage of the onshore converter, R is the equivalent resistance of the HVDC link, B is the number of the 6-pulse diode rectifier, and N is the ratio of the transformer. According to (3), V_F is linear with V_{Rdc} and I_{dc} , and the diode rectifier conducts only when V_F is higher than the threshold value because V_{Rdc} must be larger than zero.

Ignoring the loss of the rectifier, the active power and reactive power is

$$\begin{cases} P_{ac} = P_{dc} = V_{Rdc} I_{dc} \\ Q_{ac} = P \tan \varphi \\ \varphi \approx \arccos V_{Rdc} / \frac{3\sqrt{6}}{\pi} B N V_F \end{cases} \quad (4)$$

From (3) and (4), the relationship between the active power and V_F is shown in Fig. 3. The V_F increases with

an increase in active power, and the amplitude of the AC voltage is only changed from 1 to 1.03 pu when the active power output of the wind farm changes from 0 to the rated value with I_{dc} being fixed. In addition, if I_{dc} is changed, the active power will also change.

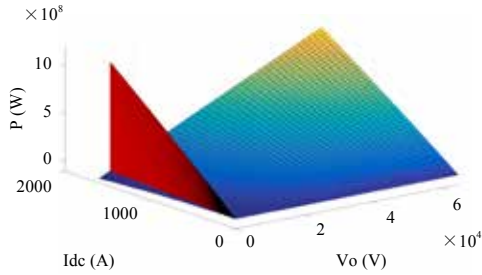


Fig. 3 Relationship among active power and AC voltage and DC current

The L_{TR} causes a commutation voltage drop in the output DC voltage. This drop can be represented as resistance r_u located at the DC side. As the commutation effect is moved to the DC side neglecting the harmonics of system, the following dq mathematical model is derived [27, 28, 32].

$$\begin{cases} V_{Rdc} = S_{1,dq}^T V_{Fdq} \\ I_{drac,dq} = S_{1,dq} I_{dc} \\ S_{1,dq} = 1.35B[\cos(\delta - \varphi), \sin(\delta - \varphi)]^T \end{cases} \quad (5)$$

where I_{drac} is the input current of the diode rectifier, δ is the angle between V_F and the d axis, and φ is the angle between V_F and I_{drac} . Note that I_{drac} can be determined by I_{dc} , which provides a new possibility for DR-HVDC.

2.3 Grid side converter of PMSG

The detailed GSC is shown in Fig. 4, where the LC filter and transformer are included. The LC filter is used to ensure a low harmonic current injection to the grid.

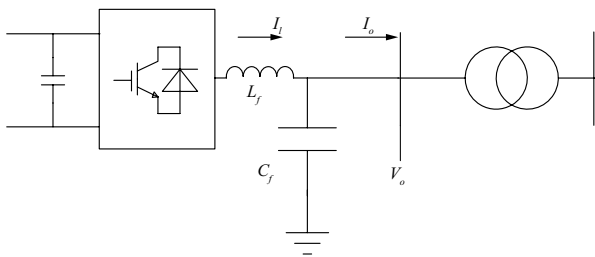


Fig. 4 Details of grid side converter

The dynamic equation of the capacitor voltage vector, inductance, and collection line expressed in the dq synchronous reference frame is

$$\begin{cases} C_f \frac{d}{dt} V_{od} = I_{ldi} - I_{od} + \omega_F C_f V_{oq} \\ C_f \frac{d}{dt} V_{oq} = I_{lqi} - I_{oq} - \omega_F C_f V_{od} \\ L_f \frac{d}{dt} I_{ldi} = -R_f I_{ldi} + \omega_F L_f I_{lqi} + V_{odi} - V_{cd} \\ L_f \frac{d}{dt} I_{lqi} = -R_f I_{lqi} - \omega_F L_f I_{ldi} + V_{oqi} - V_{cq} \\ L_L \frac{d}{dt} I_{ldi} = -R_L I_{Fdi} + \omega_F L_L I_{Fqi} + V_{odi} - V_{Fd} \\ L_L \frac{d}{dt} I_{lqi} = -R_L I_{Fqi} - \omega_F L_L I_{Fdi} + V_{oqi} - V_{Fq} \end{cases} \quad (6)$$

where C_f is the filter capacitor, V_o is the output voltage, I_o is the output current of GSC, and I_f is the current of filter inductance. Further, R_f and L_f are the respective equivalent resistance and inductance, V_{cdq} is the modulation voltage of converter, R_L and L_L are the respective equivalent resistance and inductance, and I_F is the current of collection line.

When the reactive compensation capacitor is considered, the angle between I_{dracd} and V_F is zero; that is, $I_{dracq} = 0$. According to (4) and (5), the equivalent circuit in the synchronously rotating dq frame is as shown in Fig. 5, which is easier to analyze and simplify. Further, the diode rectifier station can be considered as a voltage-dependent current source.

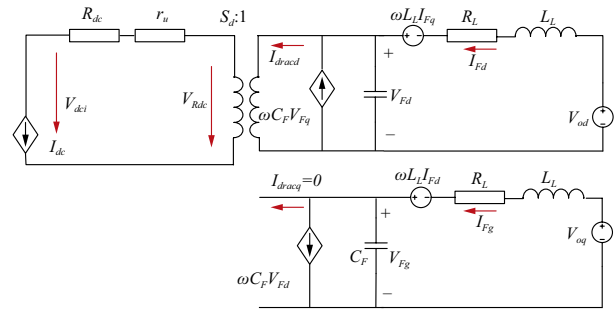


Fig. 5 Simplification of equivalent circuit considering $I_{dracq} = 0$

3 Control strategy for stability operation of offshore wind farm integrated with DR-HVDC

3.1 Control strategy of onshore converter

1) DC link current control

According to (3), the onshore converter can be operated as a voltage source or a current source.

The control of the dc-link current is illustrated in Fig. 6. A close loop is used to regulate the dc-link current I_{dc} to its reference I_{dcref} , and to generate the DC voltage reference V_{dcref} . The DC fault can be cleared by setting I_{dcref} to zero without blocking MMC if a DC fault occurs. The sub-

model voltage v_c is controlled to its reference value (v_{c_ref}) by adjusting the active power current I_d . The reactive power Q is regulated to its reference Q_{ref} . Current vector control is used to regulate the AC current I_{dq} of MMC to its reference I_{dqref} and to generate the AC voltage reference U_{abc} . A circulating current is used to optimize the converter properties and generate common-mode voltage reference u_{acmref} ; it is not illustrated here.

2) Start up

According to (4), V_{Rdc} will increase with the power transmitted by DR-HVDC with a fixed I_{dc} and V_F . To accelerate the AC voltage and decrease the power losses caused by the smaller the DC link current, a start up strategy for FBMMC is used.

$$I_{dc}^{ref} = \frac{P_{ac}}{V_{dcN}} \quad (7)$$

where V_{dcN} is the nominal DC voltage of the onshore converter.

3) Onshore fault protection

Once an onshore fault occurs, the MMC will not be able to deliver active power to the load. In general, the DC capacitor will be charged, and the DC voltage will rise rapidly because the offshore wind farm will keep delivering power.

However, the dc-link current is controlled in this study. Once the AC fault occurs, the current loop in Fig. 6 will saturate, and it would make the sub-model voltage controller invalid. The DC capacitor will then be charged, and the sub-model voltage will increase, while the DC voltage remains almost unchanged because the linear relationship between DR and the AC voltage is controlled by WT. It is difficult for offshore wind farm to detect the onshore fault without communication as no obvious local variables can be detected. And semiconductor devices will be destroyed without an additional protection strategy. Here, a protection strategy for the onshore fault is proposed.

$$I_{dc}^{ref} = \begin{cases} 1pu & \text{steady operation} \\ 1 - k_c(v_c - v_{c_{ref}})pu & \text{onshore fault} \end{cases} \quad (8)$$

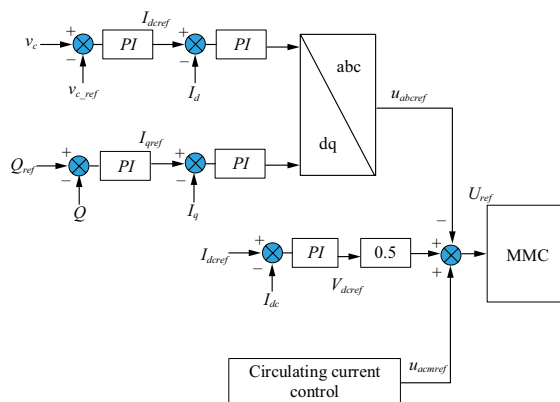


Fig. 6 Control block for onshore MMC converter

3.2 Control strategy of GSC

As mentioned before, the offshore wind turbines take the responsibility of voltage and frequency control, and power control. A simpler and faster controller of the grid-side converter of PMSG is proposed for GSC considering the onshore converter:

1) Power controller

Because the WT cluster is usually connected with parallel wind power systems, there should be a coordinated control strategy between the WTs to supply the required power without any communications among converters; therefore, droop controls are implemented [11,30].

The instantaneous active and reactive power are calculated as

$$\begin{cases} p = v_{od}i_{od} + v_{oq}i_{oq} \\ q = -v_{od}i_{oq} + v_{oq}i_{od} \end{cases} \quad (9)$$

To gain a higher quality of power being injected into grid, a one-order low-pass filter with a cut-off frequency ω_c is used [30–31]. The average active P and reactive power Q are obtained as

$$\begin{cases} P = \frac{\omega_c}{s + \omega_c} p \\ Q = \frac{\omega_c}{s + \omega_c} q \end{cases} \quad (10)$$

According to (10), the power droop control are intrinsically low band-width controllers with slow dynamics [33–34]. When voltage orientation is considered, the active power is proportional with i_{od} , and the reactive power is proportional with the i_{oq} .

At the steady state, the relationship of the output voltage of the GSC, the ac voltage at the collection point and the current can be derived from (6).

$$\begin{cases} R_L I_{Fdi} - \omega_F L_L I_{Fqi} = V_{odi} - V_{Fd} \\ R_L I_{Fqi} + \omega_F L_L I_{Fdi} = V_{oqi} - V_{Fq} \end{cases} \quad (11)$$

Equation (11) implies that the I–V characteristics of the converter that I_{Fdi} and I_{Fqi} are related to the output voltage of the converter because V_F is clamped by the diode rectifier according to (3). Therefore, power sharing between converters can be achieved by adjusting the output voltage of converters.

The power flow of the collection line can be rewritten as

$$\begin{aligned} \dot{V}_o &= V_F + \frac{PR_L + QX_L}{V_F} + j \frac{PX_L - QR_L}{V_F} \\ &= V_{Fd} + (I_{od}R_L - \omega_F L_L I_{oq}) + j(\omega_F L_L I_{od} + I_{oq}R_L) \end{aligned} \quad (12)$$

As I_{oq} is very small, it can be found that the output voltage of GSC is determined by I_{od} , and the frequency is

related to the voltage difference of the q component. To achieve faster dynamics, the I-V based droop controller is adapted here according to (11) and (12).

$$\begin{cases} V_{o-ref} = V_{oN} + K_p(I_{ld}^* - I_{ld}) + \frac{K_i}{s}(I_{ld}^* - I_{ld}) \\ \omega_{F-ref} = \omega_{FN} + K_q(I_{lq}^* - I_{lq}) \end{cases} \quad (13)$$

where I_{ld}^* is the reference value of the d-axis current and it is calculated by P_{mpp}/V_o ; I_{ld}^* is the reference of reactive power and it is designed to be zero, where V_{o-ref} is reference value of AC offshore voltage; V_{oN} is the rated value; ω_{FN} is rated frequency value; and K_q is the droop coefficient that is selected based on the power rating of wind turbines to avoid current circulation.

This I-V droop controller simplifies the nonlinear control problem of the active and reactive sharing, and it will not influence by the parameters of the line, which decouples reactive and active powers further. In addition, with the inherent filter of the active and reactive power measurement being eliminated, the system reacts quickly to power changes.

2) Voltage controller

According to (6), the open-loop output-voltage dynamics can be derived as

$$s^2 L_f C_f V_o + s C_f R_f V_o + (s L_f + R_f) I_o = V_c - V_o \quad (14)$$

As the I-V controller is used, a single-loop voltage controller is adopted without the current controller for simplification. Equation (14) shows that the output voltage belongs to a second-order system. To achieve good tracking of the output voltage, we propose the following controller expression.

$$\begin{cases} V_{cd-ref} = K_{vp}(V_{od-ref} - V_{od}) + \frac{K_{vi}}{s}(V_{od-ref} - V_{od}) + K_{vd}s(V_{od-ref} - V_{od}) \\ V_{cq-ref} = K_{vp}(V_{oq-ref} - V_{oq}) + \frac{K_{vi}}{s}(V_{oq-ref} - V_{oq}) + K_{vd}s(V_{oq-ref} - V_{oq}) \end{cases} \quad (15)$$

For a 100 MW wind farm with parameters as listed in Table 1, the PID parameters of the voltage loop are $K_{vp} = 1$, $K_{vi} = 100$, and $K_{vd} = 0.0001$. Considering only the d-axis, the control block diagram and bode plot of the transfer function is shown in Fig. 7 and 8. The system shows a gain margin of infinity and a phase margin of 32° with a bandwidth of 1030 Hz.

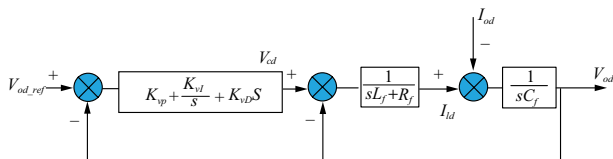


Fig. 7 Control block of AC voltage

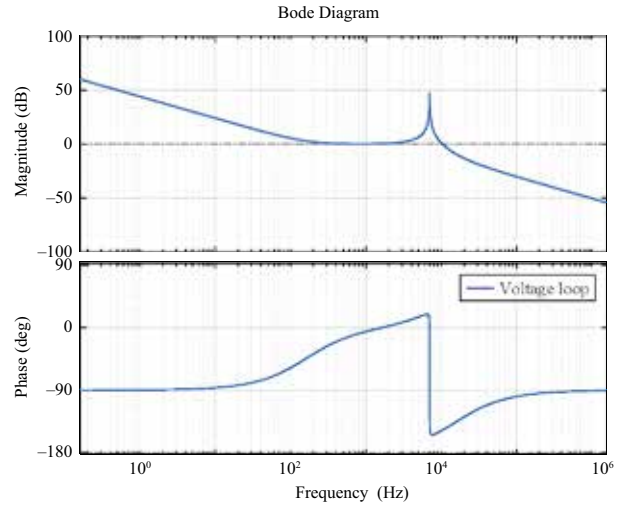


Fig. 8 Bode analysis for the voltage controller

3) Frequency controller

The three phase utility voltages can be rewritten in the synchronous reference frame using the PLL output θ^* as

$$\begin{bmatrix} V_d \\ V_q \end{bmatrix} = V_m \begin{bmatrix} \cos(\theta - \theta^*) \\ \sin(\theta - \theta^*) \end{bmatrix} \quad (16)$$

The difference of the angle is very small; therefore, the equation can be rewritten as

$$\begin{cases} V_{od-ref} \approx V_m \\ V_{oq-ref} \approx V_m(\theta - \theta^*) \end{cases} \quad (17)$$

The angle is the integration of frequency, that is,

$$V_{oq-ref} = (K_p + \frac{K_i}{s})(\omega_F - \omega_{F-ref}) \quad (18)$$

A PI controller is designed for frequency control. A new control strategy is proposed; this strategy combines droop control and Park transformation, and it is easy to design and is closer to the natural characteristics of the droop, as shown by (18).

For the 100-MW wind farm with parameters as listed in Table 1, the PI parameters of frequency loop and PLL are $K_{wp} = 42$ and $K_{wi} = 2$, and $K_{pPLL} = 0.05$ and $K_{iPLL} = 1.5$, respectively. Considering only the q-axis, the control block diagram and bode plot of the open loop is shown in Fig. 9 and 10. It can be found that the system has a gain margin of infinity and a phase margin of 170° with a bandwidth of 100 Hz. Therefore, it can be concluded that the system remains stable in the q-axis.

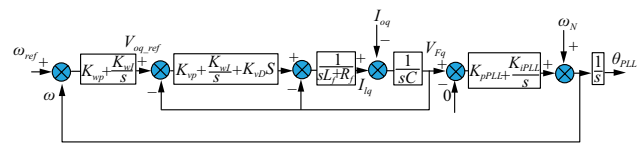


Fig. 9 Block diagram of the frequency control system

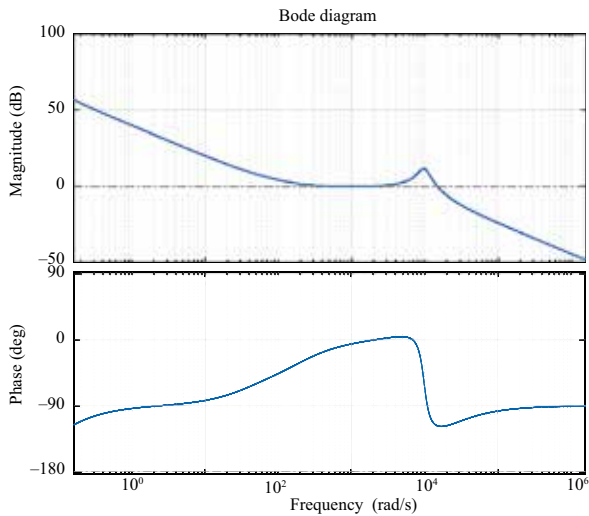


Fig. 10 Bode analysis for the frequency controller

4) Fault protection

Unlike synchronous generators, the converter does not have any overload capability, and therefore, a large transient current caused by disturbances can damage the valves during the offshore fault. Therefore, a fault protection strategy must be implemented in the control system. Once an overcurrent is detected, the current can be limited by quickly decreasing the voltage reference as shown in (19). The current will be limited as the voltage drop between the output point of the converter and the fault point is decreased.

$$\begin{cases} V_{oN}' = V_{oN} - k_{v1} |I_{od} - I_{odN}| & I_{od} > I_{odN} \\ V_{oN}' = V_{oN} - k_{v2} (V_o - V_{oN}) & V_o > V_{odN} \end{cases} \quad (19)$$

In addition, considering frequency control during the fault and to gain a faster recovery after the fault, the frequency axis, i.e., the q-axis, is kept prior, that is,

$$\begin{cases} V_{oq\max} = |V_{o\max}| \\ V_{od\max} = \sqrt{V_{o\max}^2 - V_{oq\max}^2} \end{cases} \quad (20)$$

In addition, if the onshore fault occurs, with the strategy of (8), the DC voltage of DR-HVDC will increase, which increases V_{os} , and here, a fast power reduction is used by the decreasing voltage reference as shown in (19).

The diagram of the control strategy proposed in this paper is shown in Fig. 11, which includes the I-V droop

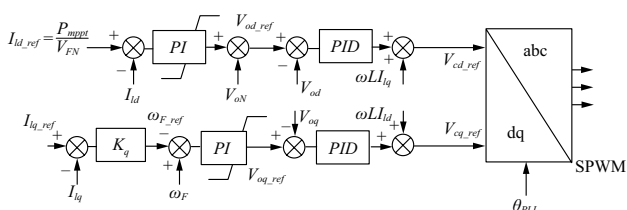


Fig. 11 Block of the controller of GSC

controller generating the voltage reference for the voltage controller and the frequency reference for the frequency controller; further, a single loop controller is used to make the output voltage track the voltage reference. As the inner loop current is eliminated, a current error-based limiter is used to protect from converter overcurrent.

4 Results

Simulation models of the HVDC system with the wind farm collected and interconnected by the diode-based rectifier are developed on the PSCAD/EMTDC platform. The topology is shown in Fig. 1, and the parameters are listed in Table 1. The string is equal to one wind power system, and there are six strings. The total rated power is 1000 MW; there are four strings rated at 200 MW and two strings rated at 100 MW. The distance between each string is 5 km. As a detailed switch mode is time consuming, an average model of the MMC is used in the simulation.

Table 1 Parameters of the simulation system

Components	Parameters	Values
Wind system	Power	200 MW/100 MW
	Transformer	3.3/66 kV
	Filter capacitor	0.1 pu
	Converter reactance	0.15 pu
	Switching frequency	1.95 kHz
Diode based Rectifier	Transformer	66/261.8/261.8 kV
	Leakage inductance	0.2 pu
Onshore VSC	DC voltage	640 kV
	DC current	1.5 kA
	Power	1000 MW
	Transformer	400 kV/330 kV

4.1 Start up and steady operation

Assume that WTs are equipped with an internal power supply such as an uninterruptible power supply (UPS) that can help the WT to supply critical components for very short durations.

The dc current of the HVDC link is built by onshore MMC first, following which the breaker of the diode rectifier and the filter are closed. The DC current of the grid-side FB-MMC is shown in Fig. 12. After the onshore FB-MMC starts up, its DC current is controlled to be 0. After 0.25 s, the DC current of the FB-MMC increases and reaches 0.32 kA. Then, the wind turbine can be started

individually, and the offshore AC voltage will be built by the GSC.

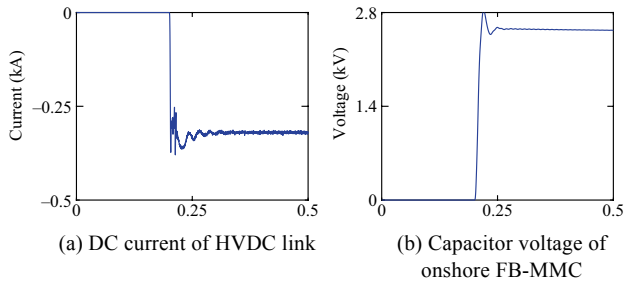


Fig. 12 Waveforms of onshore FB-MMC during startup

The self-startup of wind turbines will work once the wind speed exceeds 4 m/s. When the generator reaches a certain speed, the pitch angle is manually adjusted to 0° from 90° at a speed of 2°/s, which is neglected in the simulation. Once the generator speed reaches the nominal speed, it will be integrated into the grid. Fig. 13 and 14 shows the start-up of the system.

From Fig. 13, it can be seen that the first wind farm is started at $t = 2.5$ s, and the AC voltage is built to 3.3 kV as shown in Fig. 13(c) and wind power rated 200 MW is transmitted to the DC grid as shown in Fig. 13(a). Then, other wind farms are synchronized and integrated into the DR rectifier one by one at $t = 4.5$ s, 6.5 s, 8.5 s, 10.5 s, and 13.5 s. With more WTs connected, the reactive power produced by wind farm #1 is reduced and shared with other wind farms according to the droop coefficient, as shown in Fig. 13(b). Fig. 14 shows the curves at collection point for the corresponding values in Fig. 13. At $t = 13.5$ s, the total power of the wind farm reaches 1000 MW as shown in Fig. 14 (a). The active power of the DR increases and the reactive power decreases.

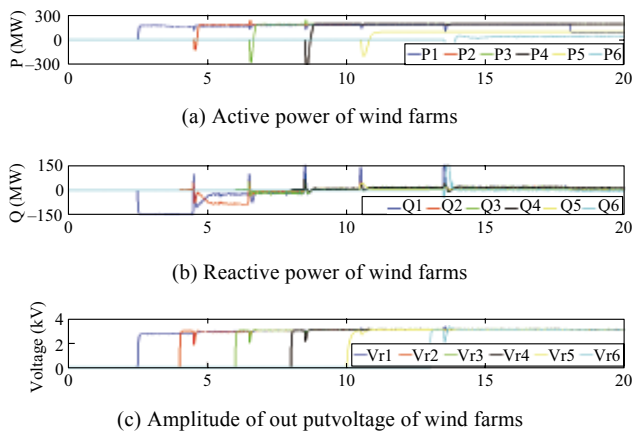


Fig. 13 Performance of the offshore system during start-up of each wind farm

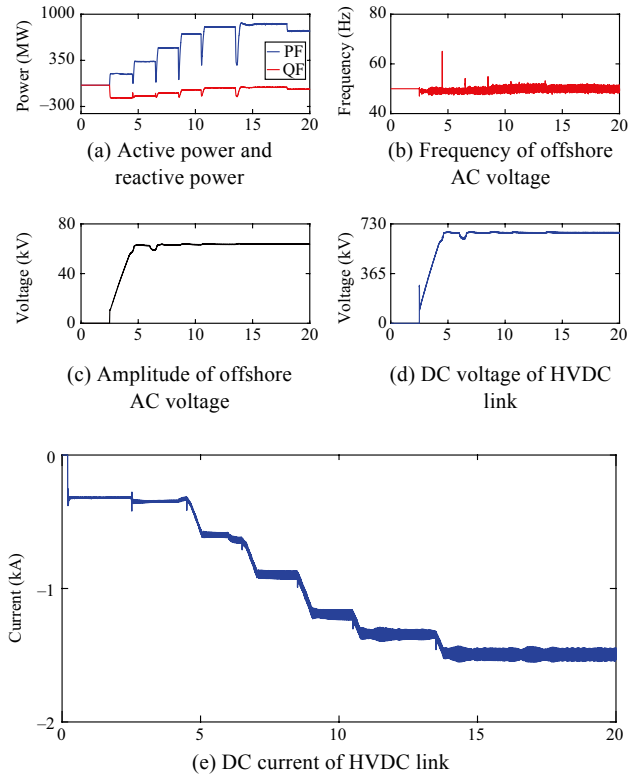


Fig. 14 Performance of the offshore system during start up and steady operation at collection point

At $t = 18$ s, the active power reference of wind farm #1 decrease from 200 MW to 100 MW, and the results shows that the output active power follows the reference. The voltage and frequency are shown in Fig. 14 (b) and (c), which maintain stable operation. The DC current of the HVDC link follows its reference as stated in (7) and as shown in Fig. 14 (e).

Note that the wind farm started first takes the responsibility of charging the transformer and the reactive compensators, and therefore, a considerable amount of reactive power will be produced by this wind farm. This reactive power is decreased once other wind farms are integrated, and it is finally shared between wind farms according to the droop coefficient.

4.2 AC Fault of offshore wind farm

A three-phase grounding fault of the offshore systems occurs at $t = 25$ s, and it lasts for 0.5 s. The AC voltage of on shore grid quickly reduces to 0, and the current of the wind farm is reduced to a small value owing to voltage protection as shown in Fig. 15. Fig. 16 and 17 show that the voltage and frequency of system and each wind farm can recover to normal quickly after the fault.

4.3 DC Fault of offshore wind farm

A permanent pole-to-pole DC fault occurs at $t = 8$ s.

The DC voltage drops to zero after the DC fault, as shown in Fig. 18 (c). The DC current control drops to 0 with the control strategy shown in Fig. 7 (b). After the DC short-circuit fault occurs, because of the coupling characteristics of the DC voltage and the AC voltage, and considering the existence of the leakage reactance of the converter

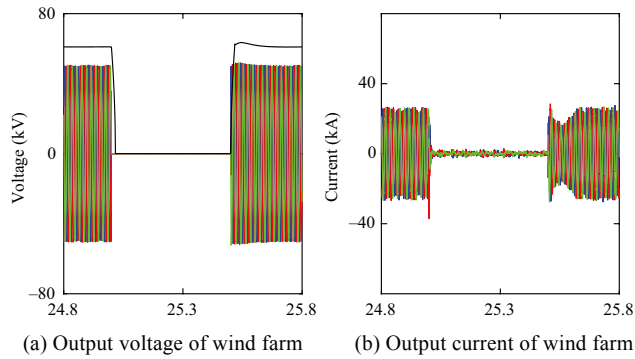


Fig. 15 Performance of the offshore system during grounding fault at collection point

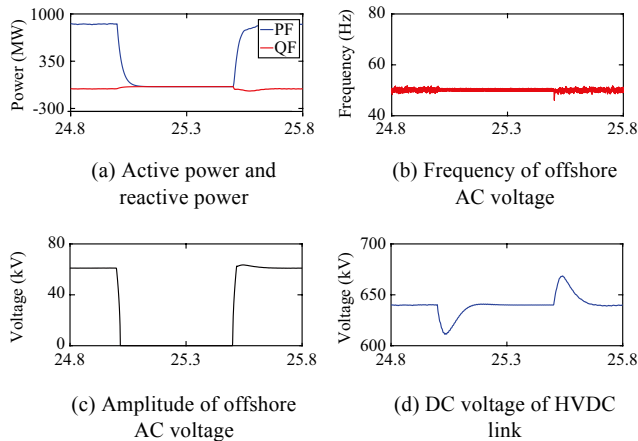


Fig. 16 Performance of the offshore system during grounding fault at collection point

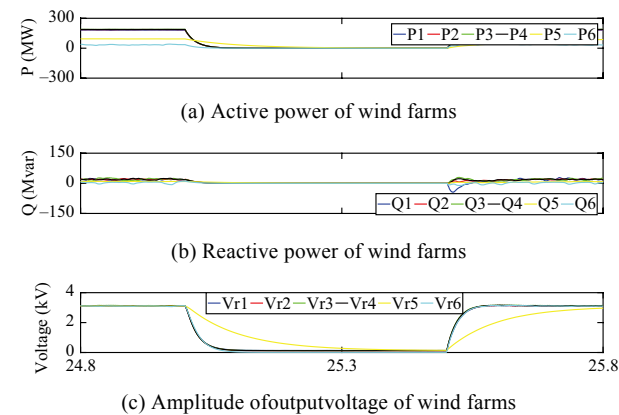


Fig. 17 Performance of each wind turbine during grounding fault at collection point

transformer, the AC voltage drops to 0.1 pu, as shown in Fig. 18 (b) and (e). That is, during the DC fault, the offshore wind farm adopts low voltage ride-through control; wind farms reduce the output power and disconnect. During the fault, the wind turbine output AC current, which is affected by the current limit control (19), is 1.2 pu, as shown in Fig. 18 (f).

4.4 AC Fault of onshore system

A three-phase grounding fault of the onshore systems occurs at $t = 4$ s and lasts 0.5 s. The AC voltage of onshore grid quickly reduces to 0 and the current of the MMC increases to its limit at about 1.2 pu as shown in Fig. 19. As shown in Fig. 19 (b), the current loop remains saturated

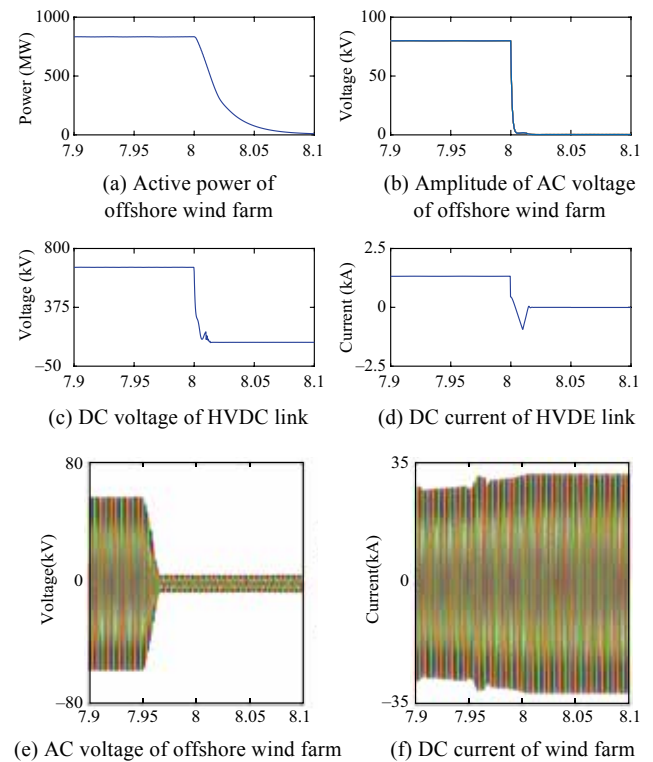


Fig. 18 Performance of the offshore system during DC fault

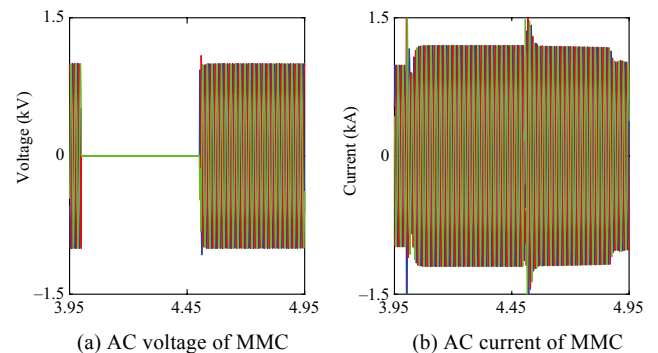


Fig. 19 Performance of MMC during onshore grounding fault

until the sub-model voltage controller returns to valid.

As onshore fault stops the transmission of the active power, and there is a difference between the active power of wind farm and the onshore system. The curves of S1 in Fig. 20 represent the case without any protection strategy. The curves of S2 in Fig. 20 represent the strategy shown in (8), and the curves of S3 represent the strategy shown in (8) and (19). The DC capacitor is charged, and the sub-model voltage increases, as shown in Fig. 20(a); the DC voltage remains constant as shown in Fig. 20 (b), which makes it difficult to detect onshore fault without communication. When the DC current reduction of S2 is adapted, the DC voltage increases as well as V_{Fs} , which makes the wind farm experience a high-voltage ride through and the active power decrease automatically. However, the overvoltage of the HVDC link is 1.4 pu. To decrease the overvoltage of the HVDC link, a fast power reduction strategy is used by the wind farm. Curves S3 show a smaller capacitor voltage, smaller DC overvoltage, and a quick response.

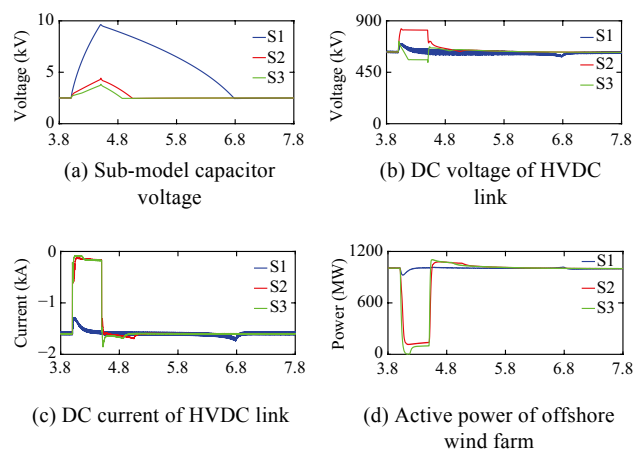


Fig. 20 Performance of the DR-HVDC during grounding fault at onshore AC grid

5 Conclusions

In this paper, a simplified strategy with a fast response is proposed for PMSG based offshore wind farms integrated with DR-HVDC.

A new coordinated control strategy for system stability operation of DR-HVDC system is proposed by analyzing the DC current control ability of the FB-MMC and characteristics of the diode rectifier, which has the advantage of flexible capability on DC fault clearing.

The relationship among voltage, frequency and current of GSC is analyzed and a simplified controller is designed based on the I-V characteristics, which has faster dynamics and more stable. A frequency controller

based on Park transformation is designed. As the DC current control of FB-MMC introduces new problem to the onshore AC fault, a protection strategy is proposed, which achieves fast onshore fault detection and power reduction to protect MMC from being destroyed without communication.

The detailed simulation model in PSCAD/EMTDC is built and various scenarios including the start-up, steady operations and response to fault are simulated. It can be concluded that the proposed control strategy can achieve the goal of synchronization of wind turbines, reactive power sharing without communications between converters, fast response once onshore or offshore fault occurs without overcurrent and overvoltage, and a quick recovery after the fault is cleared.

Acknowledgements

The work was supported by State Grid Science and Technology Project “Study on Key Technologies of Large Scale Offshore Wind Power Integrating with Onshore Grid” (4000-202055045A-0-0-00).

References

- [1] Andersen BR, Xu L (2004) Hybrid HVDC system for power transmission to island networks. *IEEE Trans Power Delivery* 19(4):1884-1890
- [2] Du C, Agneholm E, Olsson G (2008) Comparison of different frequency controllers for a VSC-HVDC supplied system. *IEEE Trans Power Delivery* 23(4):2224-2232
- [3] Du C, Bollen MH, Agneholm E, Sannino A (2007) A new control strategy of a VSC-HVDC system for high-quality supply of industrial plants. *IEEE Trans Power Delivery* 22(4):2386-2394
- [4] Torres-Olguin RE, Molinas M, Undeland T (2012) Offshore wind farm grid integration by VSC technology with LCC-based HVDC transmission. *IEEE Trans Sustainable Energy* 3(4):899-907
- [5] Liu B, Xu J, Torres-Olguin RE, Undeland T (2010) Faults mitigation control design for grid integration of offshore wind farms and oil & gas installations using VSC HVDC. Paper presented at power electronics electrical drives automation & motion, IEEE, 2010
- [6] Karaagac U, Mahseredjian J, Cai L, Saad H (2016) Offshore wind farm modeling accuracy and efficiency in MMC-based multi-terminal HVDC connection. *IEEE Trans Power Delivery* 32(2):617-627
- [7] Kallamadi M, Sarkar V (2017) Enhanced real-time power balancing of an AC microgrid through transiently coupled droop control. *IET Gener Transm Distrib* 11(8):1933-1942
- [8] De Brabandere K, Bolsens B, Van den Keybus J, Woyte A, Driesen J, Belmans R (2007) A voltage and frequency droop control method for parallel inverters. *IEEE Trans Power Electron*

- 22(4):1107-1115
- [9] Alizadeh E, Birjandi AM, Hamzeh M (2017) Decentralised power sharing control strategy in LV microgrids under unbalanced load conditions. *IET Gener Transm Distrib* 11(7):1613-1623
- [10] Rocabert J, Luna A, Blaabjerg F, Rodriguez P (2012) Control of power converters in AC microgrids. *IEEE Trans power Electron* 27(11):4734-4749
- [11] Sahoo SK, Sinha AK, Kishore NK (2017) Control techniques in AC, DC, and hybrid AC-DC microgrid: A review. *IEEE J Emerging and Selected Topics in Power Electron* 6(2):738-759
- [12] Kaviri SM, Pahlevani M, Jain P, Bakhshai A (2017) A review of AC microgrid control methods. Paper presented at 2017 IEEE 8th international symposium on power electronics for distributed generation systems (PEDG), IEEE, Florianopolis, 2017, pp. 1-8
- [13] Belenguer E, Vidal R, Beltran H, Blasco-Gimenez R (2013) Control strategy for islanded operation of offshore wind power plants connected through a VSCHVDC link. Paper presented at IECON 2013-39th annual conference of the IEEE industrial electronics society, 2013
- [14] Oriol GB, Aragüé-Peñalba M (2016) Operation and control of offshore wind power plants, Wiley-IEEE Press
- [15] Belenguer E, Vidal R, Blasco-Giménez R, Beltran H, Alfonso JC, Ariño C (2013) Islanded operation and control of offshore wind farms connected through a VSC-HVDC link. Paper presented at international conference on renewable energies and power quality, 1, 2013
- [16] Menke P et al. (2015) 2nd generation DC grid access for large scale offshore wind farms. Paper presented at proceedings of the 14th wind integration workshop, Brussels, Belgium, 2015
- [17] Blasco-Gimenez R, Ano-Villalba S, Rodríguez-D'Herle J, Morant F, Bernal-Perez S (2010) Distributed voltage and frequency control of offshore wind farms connected with a diode-based HVDC link. *IEEE Trans Power Electron* 25(12):3095-3105
- [18] Bernal-Perez S, Ano-Villalba S, Blasco-Gimenez R, Rodriguez-D'Herle J (2012) Efficiency and fault ride-through performance of a diode-rectifier-and VSC-inverter-based HVDC link for offshore wind farms. *IEEE Trans Ind Electron* 60(6):2401-2409
- [19] Seman S, Zurowski R, Taratoris C (2015) Interconnection of advanced Type 4 WTGs with diode rectifier based HVDC solution and weak AC grids. Paper presented at proceedings of the 14th wind integration workshop, Brussels, Belgium, 2015
- [20] Prignitz C, Eckel HG, Knaak HJ (2016) Voltage and current behavior in a FixReF controlled offshore wind farm using a HVDC transmission system based on uncontrolled diode rectifier units. Paper presented at 2016 18th European conference on power electronics and applications, Karlsruhe, 2016
- [21] Prignitz C, Eckel HG, Achenbach S, Augsburg F, Schön A (2016) FixReF: A control strategy for offshore wind farms with different wind turbine types and diode rectifier HVDC transmission. Paper presented at 2016 IEEE 7th international symposium on power electronics for distributed generation systems (PEDG), 2016
- [22] Herrera D, Galván E, Carrasco JM (2017) Method for controlling voltage and frequency of the local offshore grid responsible for connecting large offshore commercial wind turbines with the rectifier diode-based HVDC-link applied to an external controller. *IET Electr Power Appl* 11(9):1509-1516
- [23] Yu L, Li R, Xu L (2018) Distributed PLL-based control of offshore wind turbines connected with diode-rectifier-based HVDC systems. *IEEE Trans Power Delivery* 33(3):1328-1336
- [24] Li R, Yu L, Xu L (2018) Offshore AC fault protection of diode rectifier unit-based HVDC system for wind energy transmission. *IEEE Trans Ind Electron* 66(7):5289-5299
- [25] Wang X, Loh PC, Blaabjerg F (2017) Stability analysis and controller synthesis for single-loop voltage-controlled VSIs. *IEEE Trans Power Electron* 32(9):7394-4704
- [26] Li X, Lin P, Tang Y, Wang K (2018) Stability design of single-loop voltage control with enhanced dynamic for voltage-source converters with a low LC-resonant-frequency. *IEEE Trans Power Electron* 33(11):9937-9951
- [27] Areerak KN, Bozhko SV, Asher GM, De Lillo L, Thomas DW (2012) Stability study for a hybrid AC-DC more-electric aircraft power system. *IEEE Trans Aerosp Electron Syst* 48(1):329-347
- [28] Areerak KN, Bozhko SV, Asher GM, Thomas DW (2008) DQ-transformation approach for modelling and stability analysis of AC-DC power system with controlled PWM rectifier and constant power loads. Paper presented at 2008 13th international power electronics and motion control conference, Poznan, 2008, 2049-2054
- [29] Deng Y, Tao Y, Chen G, Li G, He X (2016) Enhanced power flow control for grid-connected droop-controlled inverters with improved stability. *IEEE Trans Ind Electron* 2016 64(7):5919-5929
- [30] An R, Liu J, Wu T, Wang S, Liu B (2017) Analysis and design of cutoff frequency for power calculation low-pass filters in droop control. Paper presented at 2017 IEEE 3rd international future energy electronics conference and ECCE Asia, Kaohsiung, 2017, 1596-1600
- [31] Wang S, Liu Z, Liu J, Boroyevich D, Burgos R (2019) Small-signal modeling and stability prediction of parallel droop-controlled inverters based on terminal characteristics of individual inverters. *IEEE Trans Power Electron* 35(1):1045-1063
- [32] Griffio A, Wang J (2012) Large signal stability analysis of 'more electric' aircraft power systems with constant power loads. *IEEE Trans Aerosp Electron Syst* 48(1):477-489
- [33] Li Y, Fan L (2017) Stability analysis of two parallel converters with voltage-current droop control. *IEEE Trans Power Delivery* 32(6):2389-2397
- [34] Pasha AM, Zeineldin HH, Al-Sumaiti AS, El Moursi MS, El Sadaany EF (2017) Conservation voltage reduction for autonomous microgrids based on V-I droop characteristics. *IEEE Trans Sustainable Energy* 8(3):1076-1085

Biographies



Lijun Xie received the BEng.degree from HEBEI University of Technology in 2012, and the M.S. degree in power electronic from China Electric Power Research Institute (CEPRI), in 2015. She is currently working toward the Ph.D. degree at CEPRI. Her research interest is large-scale renewable energy integration by DC grid.



Liangzhong Yao received the M.S and Ph.D degrees in electrical engineering from Tsinghua University, Beijing, China, in 1989 and 1993 respectively. Then, he joined the Institute of Nuclear and New Energy Technology of Tsinghua University, as an Associate Professor from 1993 to 1995, and completed Postdoctoral research in the

University of Manchester from 1995 to 1999. After that, he worked as a Senior Power System Analyst in ABB from 1999 to 2004, and a Senior Expert and Technical Adviser in Alstom Grid until 2011. From 2012 to 2017, he served as Associate Dean of China Electric Power Research Institute. He is currently a Professor of Wuhan University, Special Expert of national talent invitation program. His current research interests include the integration technology of large-scale renewable energy, analysis of characteristics of DC-based renewable energy sources, control and operation of DC grids, DC transmission technologies, and key technologies of DC equipments. He has published over 200 journal papers, 5 book chapters, and held 10 patents. He is the Chairman of IEC TC122 and the Convener of IEC TC8 JWG10. He is an IET Fellow, and an Associate Editor of CSEE Journal of Power Energy & System and IET Journal of High Voltage. He is also a Member of Editorial Board of Journal of IET Renewable Power Generation, Journal of Modern Power Systems and Clear Energy, Frontier in Energy, Proceedings of the CSEE and Power System Technology.



Fan Cheng received the B.S. degree in electric engineering and automation from South China University of Technology, Guangzhou, Guangdong province, China in 2010 and the M.Eng. degree in electric engineering from Southeast University, Nanjing, Jiangsu province, China, in 2014. He is currently pursuing the Ph.Eng. degree in electric engineering at China electric power research institute, Beijing, China. His research interest includes the high voltage direct current technology, large scale renewable energy integration and interaction stability analysis of electronic power system.



Yan Li received his B.S. degree from Shandong University of Technology in 1999, and received his M.S. degree from Fuzhou University in 2002, and received his Ph.D. degree from China Electric Power Research Institute (CEPRI) in 2007. Since 2007 he has been employed at CEPRI, presently as Renewable Energy Integration modeling and Simulation Research Division director of Renewable Energy Department of CEPRI. His interested researches are the power system analysis, renewable energy modeling and grid integration simulation, renewable energy develop planning.



Shuai Liang received the B.S. and M.S. degrees in electrical engineering from Northeast Electric Power University, China, in 2015 and 2019. He is currently working toward the Ph.D. degree in Wuhan University. His research interests include renewable energy conversion systems and transient stability analysis.

(Editor Dawei Wang)